Comparison of PM Motor Structures and Sensorless Control Techniques for Zero-Speed Rotor Position Detection

Nicola Bianchi, *Member, IEEE*, Silverio Bolognani, *Member, IEEE*, Ji-Hoon Jang, *Student Member, IEEE*, and Seung-Ki Sul, *Fellow, IEEE*

***Abstract*—The rotor position of a synchronous permanent magnet (PM) motor can be detected by means of the injection of a high-frequency stator voltage superimposed to the fundamental component. Thanks to the rotor anisotropy, the corresponding high-frequency current is modulated and used to determine the rotor position. Two techniques are considered: the first one adopts a pulsating voltage vector in the estimated synchronous reference frame, while the second one adopts a rotating voltage vector. These techniques are effective at zero and at low motor speed. The accuracy of the rotor position detection depends strictly on the rotor saliency, that is, on the geometry of the PM rotor. In fact both saturation and d- and q-axis cross-coupling have a heavy influence on the correct rotor position detection.**

The aim of this paper is to compare the two sensorless control techniques, together with two rotor geometries, that is, IPM and inset rotor. In order to highlight the effectiveness of the sensorless technique, the tests are carried out at various operating conditions. It is found that the effectiveness of the sensorless rotor position detection strongly depends on the PM rotor geometry. Conversely, the choice of the sensorless control technique affects slightly the rotor position detection.

***Index Terms*—High-frequency signal injection, interior permanent magnet (PM) motor, low-speed sensorless control, motor design optimization, zero-speed sensorless control.**

I. Introduction

At low and zero speed, the sensorless techniques based on the back EMF detection cannot be used [1]–[3], thus, sensorless position control techniques are based on the rotor angle identification based on the rotor saliency [4], [5] that is a key property of a class of synchronous permanent magnet (PM) machines [6]–[11]. To this purpose, a high-frequency stator voltage is superimposed to the fundamental voltage component. The rotor saliency affects the magnitude of the high-frequency stator current, from which the rotor position can be identified [12]–[17]. Since this technique is based on the PM rotor saliency, the accuracy of the rotor position detection depends strictly on the rotor geometry. The effectiveness of the technique can be limited to part loads by iron saturation (where stator currents are limited). In addition, the magnetic cross-coupling between d-axis and q-axis [18], [19] has a heavy influence on the correct rotor position detection [20], [21].

The aim of this paper is to compare two sensorless control techniques based on the injection of a high frequency signal, in order to verify if one is more effective than the other.

Several tests are carried out at various operating conditions, so as to consider both saturation and d- and q-axis cross-coupling effects. Two PM motors with completely different rotor geometries are tested, so as to investigate the more suitable configuration for zero-speed sensorless control.

The result of this paper is to highlight which is the influence of the control technique as well as of the PM rotor geometry, on the accuracy of the sensorless rotor position detection.

II. Techniques Based on Superimposition of a High-Frequency Voltage Vector

When the high-frequency stator voltage is added to the fundamental voltage, the corresponding high-frequency stator current is affected by the rotor saliency [1], [22]–[24]. Therefore, information of the rotor position is extracted from current measurement [25], [26]. The two techniques used to detect the PM rotor position by means of high-frequency signal injection, are briefly summarized hereafter.

Let

$$L_{\text{avg}} = \frac{L_{qh} + L_{dh}}{2} \quad \text{and} \quad L_{\text{dif}} = \frac{L_{qh} - L_{dh}}{2} \tag{1}$$

be the average and difference inductances of the high-frequency motor model. Taking into account the saturation, the inductances vary according to the actual operating point. Referring to the high-frequency motor model, the d- and q-axis inductances in (1) are the incremental inductances (also called dynamic or differential inductances), corresponding to the actual operating point.

A. Pulsating Voltage Vector Technique

A pulsating voltage vector is superimposed along the estimated d-axis at a constant carrier frequency ω_h. In the estimated

Manuscript received July 14, 2006; revised December 19, 2006. This paper was presented at the IEEE Power Electronic Specialists Conference, PESC'05, Jeju, Korea, June 18–22, 2006. This work was supported by the Electric Drive Laboratory, Department of Electrical Engineering, University of Padova, Italy and by Magnetic S.p.a., Montebello Vicentino, Italy. Recommended for publication by Associate Editor A. Consoli.

N. Bianchi and S. Bolognani are with the Department of Electrical Engineering, University of Padova, Padova I-35131, Italy (e-mail: bianchi@die.unipd.it; bolognani@die.unipd.it).

J.-H. Jang is with the HEV System Engineering Team, Corporate Research and Development Division, Hyundai Motor Company, Gyeonggi-Do 472-936, Korea (e-mail: jihoon.jang@hyundai-motor.com).

S.-K. Sul is with the School of Electrical Engineering, and Computer Science, Seoul National University, Seoul 110-744, Korea (e-mail: sulsk@plaza.snu.ac.kr).

Digital Object Identifier 10.1109/TPEL.2007.904238

0885-8993/$25.00 © 2007 IEEE

synchronous reference frame $\tilde{d}-\tilde{q}$, such a voltage vector is given by

$$\begin{aligned}\tilde{v}_{dh} &= V_h \cos(\omega_h t)\\ \tilde{v}_{qh} &= 0\end{aligned} \tag{2}$$

where the superscript $\sim$ means that the vector is in the estimated reference frame. The corresponding high-frequency current components can be expressed as

$$\begin{aligned}\tilde{i}_{dh} &= \frac{V_h}{\omega_h L_{dh} L_{qh}} \left[L_{\text{avg}} + L_{\text{dif}} \cos(2\vartheta^e_{\text{err}})\right] \sin(\omega_h t)\\ \tilde{i}_{qh} &= \frac{V_h}{\omega_h L_{dh} L_{qh}} \left[L_{\text{dif}} \sin(2\vartheta^e_{\text{err}})\right] \sin(\omega_h t)\end{aligned} \tag{3}$$

where a rotor speed $\omega^e_m = 0$ is fixed for the sake of simplicity. In (3), ϑ^e_{err} is the electrical angle error between the estimated $\tilde{d}-\tilde{q}$ and the actual $d-q$ synchronous reference frame.

Equation (3) shows that high-frequency component of q-axis current in the estimated rotor reference frame becomes zero when the rotor position angle error is zero. Thus only q-axis component could be processed as follows, obtaining the rotor position estimation error signal $\varepsilon(\vartheta^e_{\text{err}})$ as

$$\varepsilon\left(\vartheta^e_{\text{err}}\right) = \text{LPF}\left[\tilde{i}_{qh} \sin(\omega_h t)\right] \tag{4}$$

where LPF means low-pass filter. It becomes

$$\varepsilon(\vartheta^e_{\text{err}}) = \frac{V_h}{\omega_h} \frac{L_{\text{dif}}}{2 L_{dh} L_{qh}} \sin(2\vartheta^e_{\text{err}}). \tag{5}$$

It can be noted that the error signal is proportional to the sine function of twice the rotor position estimation error. However, it is important to observe that the information of the rotor position strongly depends on the difference inductance L_{dif}. The error signal disappears when $L_{dh} = L_{qh}$.

B. Rotating Voltage Vector Technique

Alternatively, a voltage vector rotating at a constant carrier frequency ω_h is superimposed to the fundamental voltage. In the stationary reference frame $\alpha-\beta$, such a voltage vector is given by

$$\mathbf{v}_{\alpha\beta h} = V_h e^{j\omega_h t}. \tag{6}$$

Neglecting the stator resistance, the corresponding high-frequency current vector is given by

$$\mathbf{i}_{\alpha\beta h} = \frac{L_{\text{avg}} \mathbf{v}_{\alpha\beta h} - L_{\text{dif}} e^{j2\vartheta^e_m} \mathbf{v}^*_{\alpha\beta h}}{j\omega_h L_{dh} L_{qh}} \tag{7}$$

where superscript * means the complex conjugate, and ϑ^e_m is the rotor position angle in electrical radians.

In order to achieve a signal related to the rotor position angle, the current vector (7) is firstly multiplied by $e^{-j\omega_h t}$ and the result is processed by means of a high pass filter (heterodyning scheme) [9], yielding

$$\text{HPF}\left[\mathbf{i}_{\alpha\beta h} e^{-j\omega_h t}\right] = j \frac{V_h}{\omega_h} \frac{L_{\text{dif}}}{L_{dh} L_{qh}} e^{j2(\vartheta^e_m - \omega_h t)}. \tag{8}$$

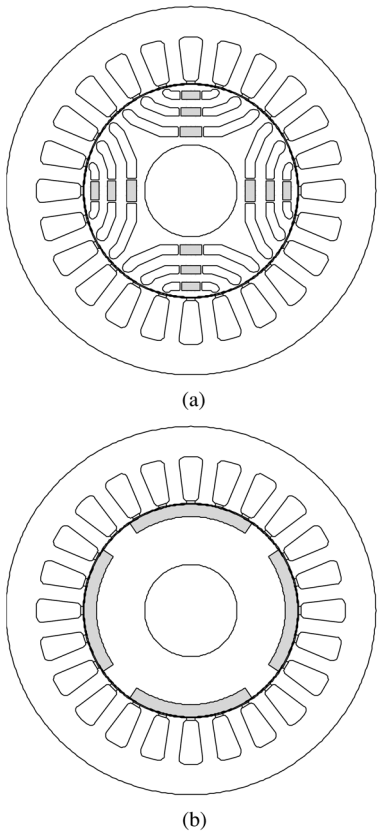

Fig. 1. PM motors with different rotors: (a) IPM rotor and (b) inset rotor.

Let $\tilde{\vartheta}^e_m$ be the estimated rotor position angle, the signal (8) is multiplied by $e^{j2(\omega_h t - \tilde{\vartheta}^e_m)}$. Then, the rotor position estimation error signal ε corresponds to the real part of such a product, which is

$$\varepsilon = -\frac{V_h}{\omega_h} \frac{L_{\text{dif}}}{L_{dh} L_{qh}} \sin\left[2\left(\vartheta^e_m - \tilde{\vartheta}^e_m\right)\right]. \tag{9}$$

Also in this case the information of the rotor position depend on the difference inductance L_{dif}.

III. Influence of the PM Rotor Structure

Saturation and d-axis and q-axis cross-coupling may affect the effectiveness of the sensorless identification, causing a considerable error in the rotor position detection [27], [28]. However, it has been proved that the design of suitable PM rotor configurations allows these disturbing phenomena to be minimized [10], [29]. To this aim, finite element (FE) analysis can be profitably carried out to investigate the impact of the rotor geometry on the accuracy of the rotor position detection [30]. Therefore, some key design rules can be established so as to maximize the effectiveness of the sensorless rotor position detection, even under heavy operating conditions.

This paper considers two PM motors with completely different rotor geometry: an interior PM (IPM) motor with three flux-barriers per pole, shown in Fig. 1(a), and an inset PM motor, shown in Fig. 1(b). The rotor of the inset motor is a surface-mounted PM rotor with iron teeth between adjacent PMs.

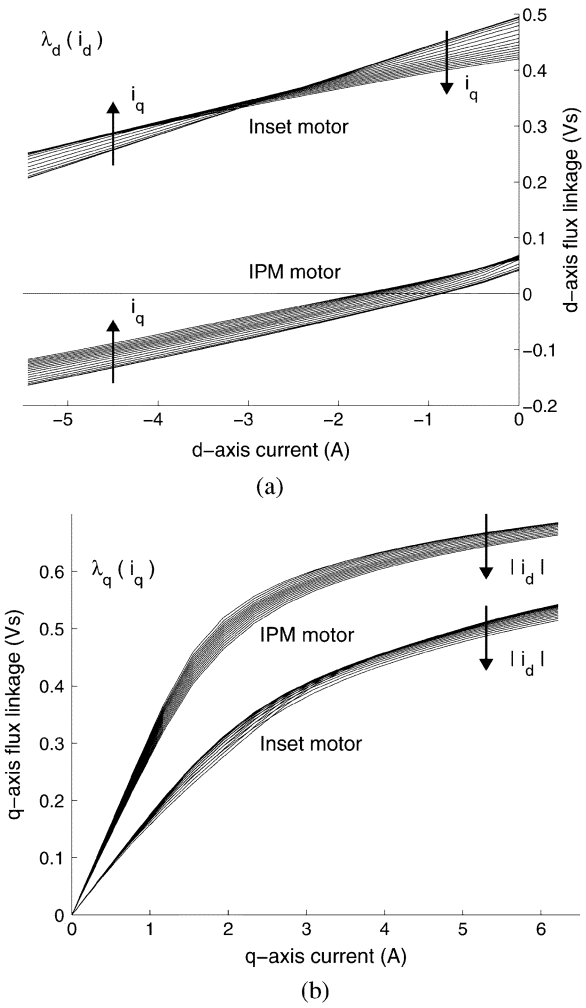

Fig. 2. d-axis flux linkage versus d-axis current (a) and q-axis flux linkage versus q-axis current (b) of IPM and inset motor of Fig. 1. (a) d-axis. (b) q-axis.

A. *Flux Linkages Versus Currents in Synchronous Reference Frame*

The flux linkage versus current characteristics of the two PM motors are derived by means of FE analysis. Such characteristics are shown in Fig. 2, according to the two motors of Fig. 1. Fig. 2(a) shows the d-axis flux linkages as a function of the d-axis currents, for different q-axis currents, and Fig. 2(b) shows the q-axis flux linkages as a function of the q-axis currents, for different d-axis currents. Magnetostatic FE simulations have been carried out with fixed rotor position. Effect of rotor skewing has been neglected. The influence of rotor position and skewing has been investigated and can be neglected to the purpose of this study.

At high q-axis current, the effect of the saturation is evident, especially for the IPM motor. This implies that the difference inductance $L_{\rm dif}$ decreases rapidly towards zero, and the rotor position detection could be unfesible at high q-axis current. Finally, let us observe that the d- and q-axis flux linkages are a function of both the d- and q-axis currents, due to the cross-coupling effect [31].

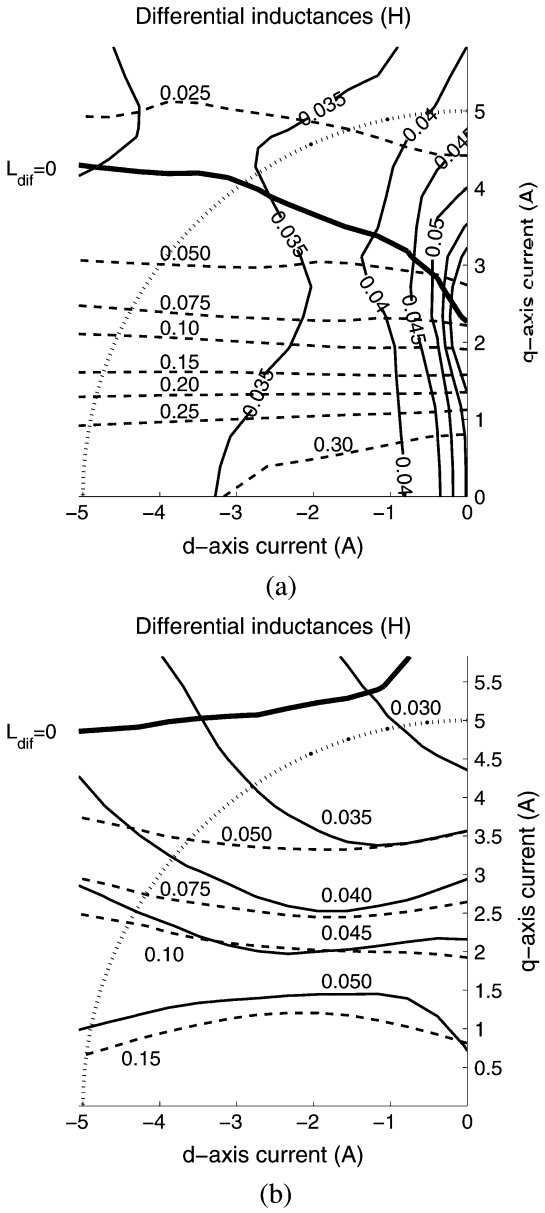

Fig. 3. Feasible region for sensorless control in the (i_d, i_q) plane (it refers to the PM motors shown in Fig. 1). (a) IPM motor. (b) Inset motor.

B. *Feasibility Region in the (i_d, i_q) Plane*

In [32], the feasible region for the sensorless rotor position detection has been defined.

In the (i_d, i_q) plane, the two-axis incremental inductances can be drawn, as shown in Fig. 3. The q-axis inductance is drawn by dashed line, while the d-axis inductance is drawn by solid line. The dotted circle arc refers to a reasonable fundamental current according to thermal considerations.

The curve defined by $L_{\rm dif} = 0$, drawn in bold line, defines the locus in the (i_d, i_q) plane in which the signal of the rotor position defined by (5) and (9) is zero, the latter being proportional to $L_{\rm dif}$, as shown by (5) and (9). The feasible region is defined as the region bounded by this curve so as to have $L_{\rm dif} > 0$.

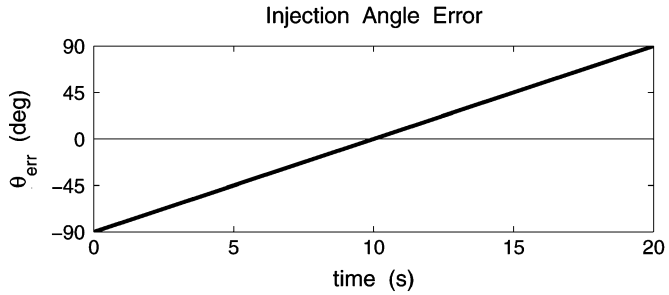

Fig. 4. Injection angle error signal varying from -90 to $90°$.

IV. Simulation Results

Both motor configurations shown in Fig. 1 are considered hereafter. The following simulation results show the error signals ε under various operating conditions. The d- and q-axis flux linkages versus currents characteristics of Fig. 2 are used to extract the incremental inductances L_{dh}, L_{qh} and $L_{\rm dif}$ for each working point. They can be inserted in (3) and (7), in order to compute the high frequency currents, and in (5) and (9) to compute the signal error. The amplitude and the frequency of injected high-frequency voltage signal are 50 V and 500 Hz, respectively.

Fig. 4 shows the rotor position angle error, that is changed from -90 to $+90°$ in a time from 0 to 20 s. All the following figures report the error signal ε, for given fundamental d- and q-axis currents and rotor speed, according to the angle error of Fig. 4. All the simulations are carried out considering a rotor speed of 0 r/min.

A. Pulsating Voltage Vector (IPM Motor Configuration)

At first, IPM motor is considered, whose magnetic characteristics are shown in Fig. 2. Fig. 5 shows the estimation error signals. When q-axis current is low [Fig. 5(a)], error signal ε varies sinusoidally as a function of twice the injection angle error, as in (5). It is worth noticing that it is zero when the injection angle error is zero.

The error signal results to be as more distorted, as the torque applied to the machine increases: increasing q-axis current, the error signal amplitude decreases and the angular displacement increases, as shown in Fig. 5(b). Then, it is severely distorted with high q-axis current amplitude, as shown in Fig. 5(c). Therefore, it can be inferred that the estimation of rotor position will be degraded severely when operating under heavy load.

When the rotor speed is 100 r/min (i.e., fundamental frequency is equal to 3.33 Hz), similar results are obtained at zero rotor speed. This similarity is due to the fact that simulations do not reflect the disturbances or nonlinearities caused by the rotor speed.

It has been verified that a negative d-axis current is advantageous for the IPM motor, and in particular for the IPM motor that is considered in this paper, since it exhibits a low PM flux. In fact, the negative d-axis current takes part in saturating the rotor iron bridges, keeping a low value of L_{dh}. From the working point defined by $I_d = 0$ A, $I_q = 0$ A to the working point defined by $I_d = -2$ A, $I_q = 0$ A the error signal $\varepsilon(\vartheta^e_{\rm err})$ increases of 80%. This does not happen by using the inset motor.

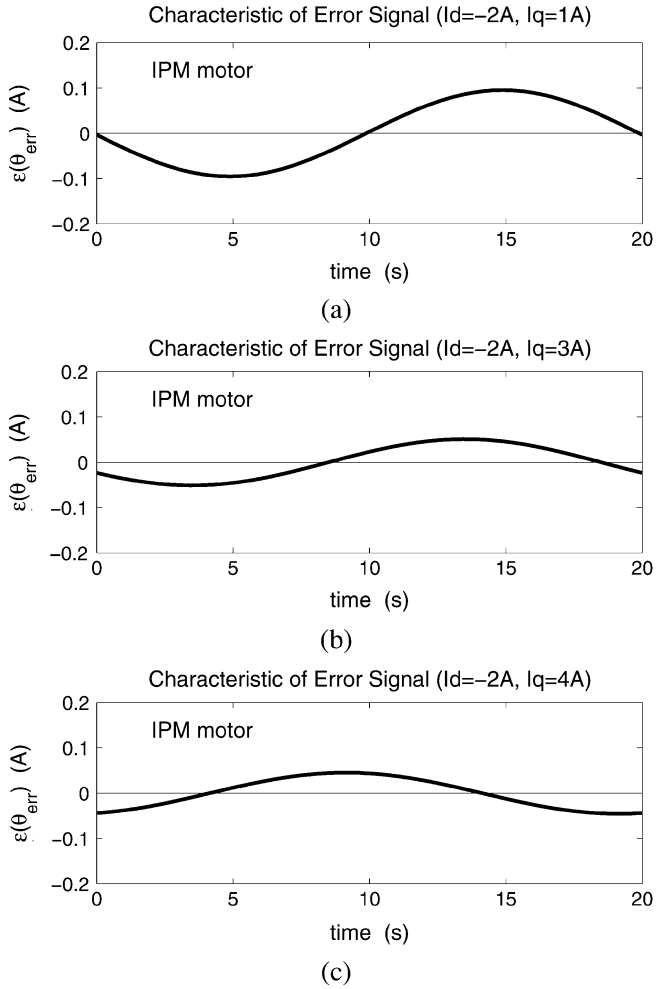

Fig. 5. IPM rotor: estimation error signal with pulsating voltage injection.

B. Rotating Voltage Vector (IPM Motor Configuration)

Fig. 6. shows the simulation results based on the rotating high-frequency signal injection method and heterodyning process. The magnitudes of the error signal under part load conditions are double than those from the pulsating high-frequency voltage signal injection method, which can be inferred by comparing (9) and (5). However, even though the magnitudes of error signal are larger in the rotating high-frequency voltage signal injection method, the distortion of the signal versus the rotor position estimation error occurs under the same load of the previous case.

C. Pulsating Voltage Vector (Inset Motor Configuration)

The same simulations have been carried out adopting the inset motor configuration. The same stator has been considered, while the rotor has been changed. The magnetic characteristics in Fig. 2 have been used in the motor model. The simulated results are shown in Fig. 7.

Fig. 7(a) and (b) show that a proper error signal is achieved at part load. Then, Fig. 7(c) shows the simulation results with fundamental currents $I_d = -2$ A and $I_q = 4$ A. It is worth noticing that the variation of the error signal ε still remains sinusoidal

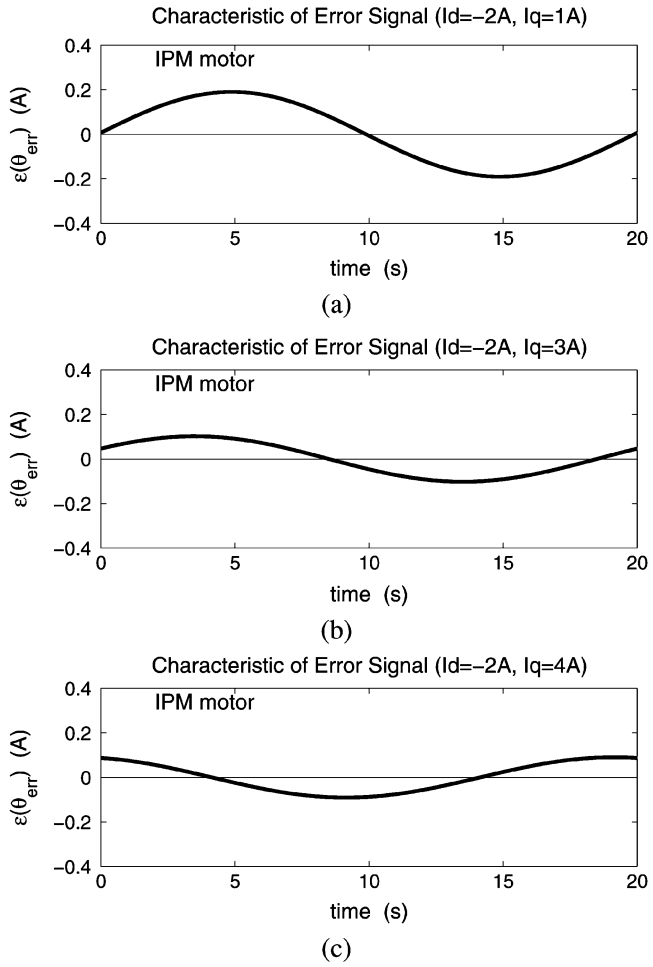

Fig. 6. IPM rotor: estimation error signal with rotating voltage injection.

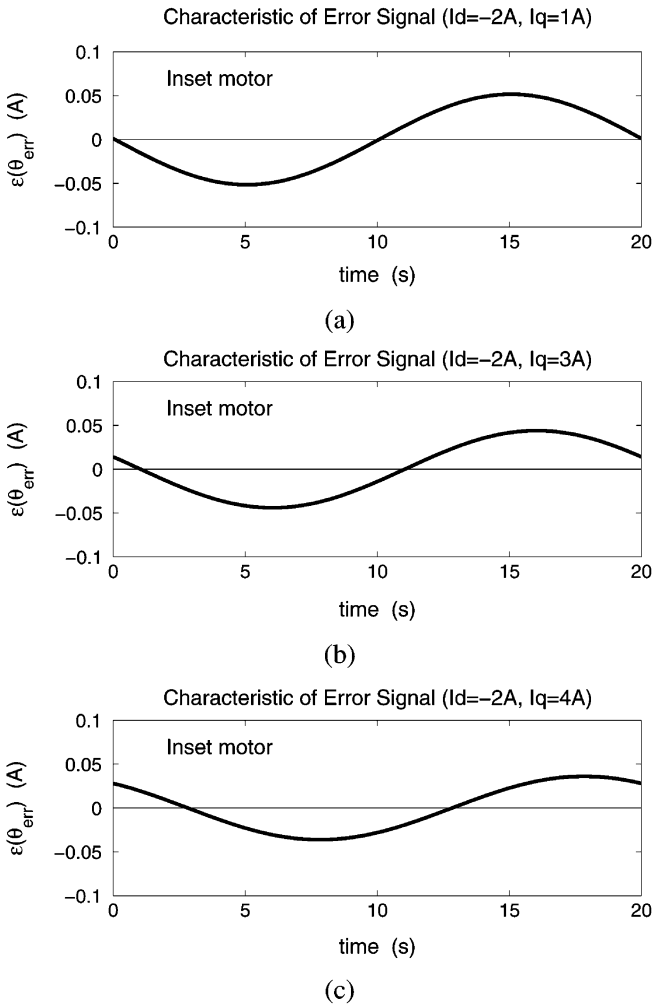

Fig. 7. Inset rotor: estimation error signal with pulsating voltage injection.

with a minimum distortion from (5), in spite of the high fundamental current amplitude. This result suggests that this rotor type allows a more accurate rotor position detection to be carried out.

D. Rotating Voltage Vector (Inset Motor Configuration)

Similar results are obtained using the rotating high-frequency signal injection method, as shown in Fig. 8.

V. Experimental Results

Both motors shown in Fig. 1 have been experimentally tested. The same stator has been adopted for the two motors, and only the rotor has been changed. The IPM rotor is characterized by three flux-barriers per pole while the inset rotor by surface-mounted PMs and a tooth covering about one stator slot, as sketched in Fig. 1.

A high-frequency voltage was injected with amplitude $V_h = 50$ V and frequency $f_c = 500$ Hz, superimposed to the fundamental voltage component. The tests were carried out at the motor speed $n = 0$ and $n = 50$ r/min. There are no appreciable differences at these two speeds.

Both rotors are laminated, limiting the eddy currents induced in the rotor by the high frequency signal injection. As a consequence, a variation of the carrier frequency has a negligible impact on the error signal.

A. Pulsating Voltage Vector (IPM Motor Configuration)

The experimental results using the pulsating voltage injection technique are shown in Fig. 9 (low current test) and Fig. 10 (high current test). Experimental test at the operating point defined by $I_d = -2$ A, $I_q = 0$ A gives a similar result, and it is not reported here.

The results confirm the simulated prediction: at the higher currents the rotor position estimation error signal becomes smaller and distorted (an error of 20° can be recognized in Fig. 10). It has also be verified that in the operating point defined by $I_d = -2$ A and $I_q = 3$ A, the error signal becomes very small with a distortion of about 30°.

Comparing Figs. 9 and 10 with Fig. 5, one can observe that the experimented behavior of the rotor position estimation error signal is similar to the predicted one. However, the amplitude of the error signal is higher in simulations than in measures. It is the authors' opinion that this is due to the FE modelling of the saturation of the rotor bridges. It has been verified that slight variations in the iron bridge saturation (e.g., due to geometrical tolerance of the rotor prototype) yield variations of more than 100% of the d-axis incremental inductance, and thus of the error signal.

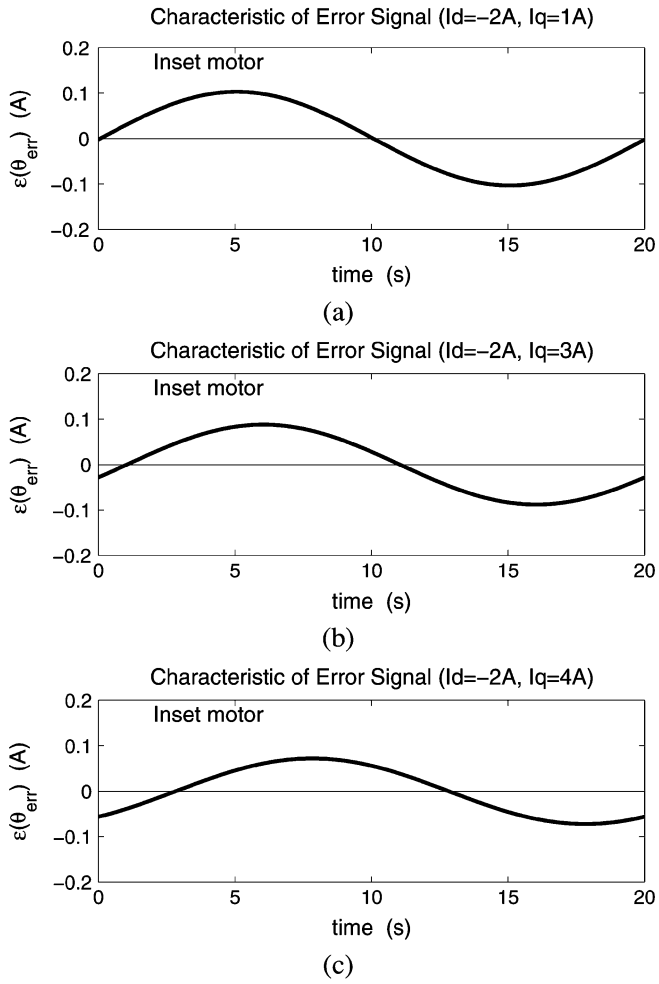

Fig. 8. Inset rotor: estimation error signal with rotating voltage injection.

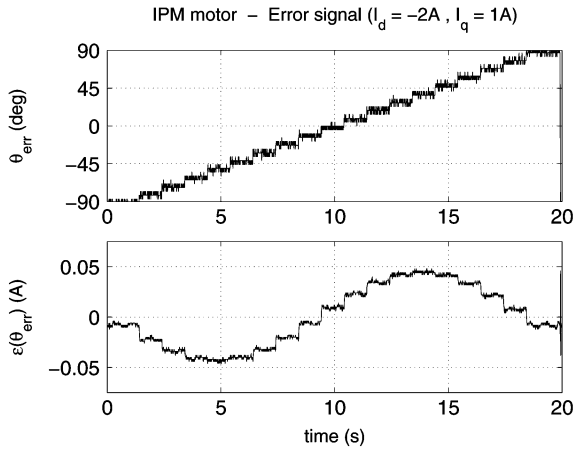

Fig. 9. IPM rotor: rotor position error and estimation error signal with pulsating voltage injection (experimental test).

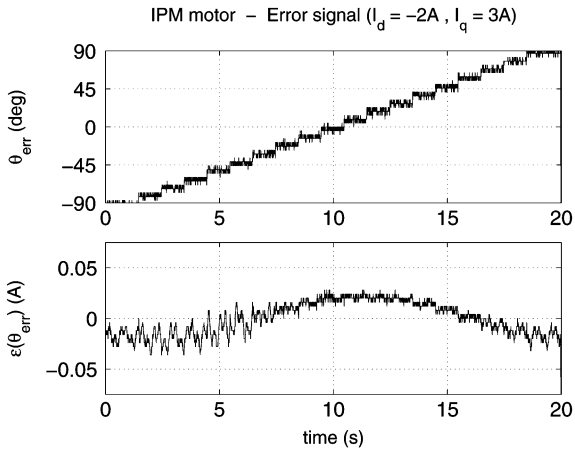

Fig. 10. IPM rotor: rotor position error and estimation error signal with pulsating voltage injection (experimental test).

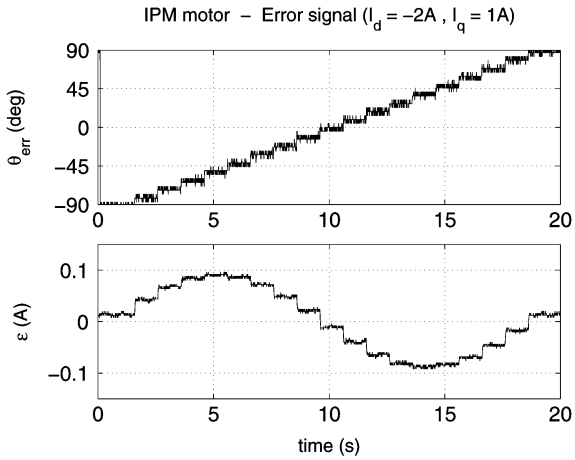

Fig. 11. IPM rotor: rotor position error and estimation error signal with rotating voltage injection (experimental test).

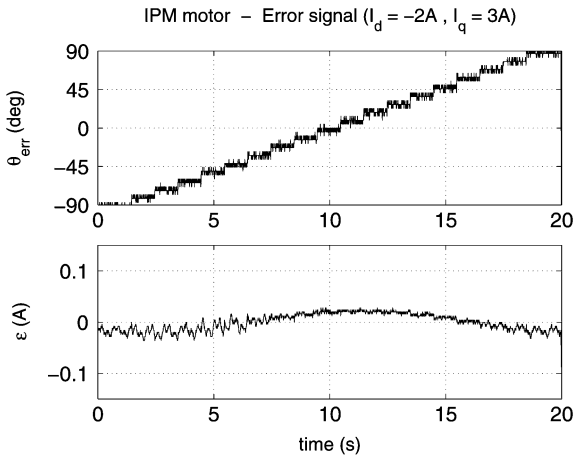

Fig. 12. IPM rotor: rotor position error and estimation error signal with rotating voltage injection (experimental test).

B. Rotating Voltage Vector (IPM Motor Configuration)

Similar results are achieved by means of the rotating voltage injection, as shown in Fig. 11 (low current test) and Fig. 12 (high current test). The rotor position estimation error signal decreases as the q-axis current increases. It has been also observed that the error signal is very distorted when the q-axis current exceeds $I_q = 3$ A so that the rotor position is hardly recognized.

As above, experimental results of Figs. 11 and 12 can be compared with those of Fig. 6. Although the amplitude of the

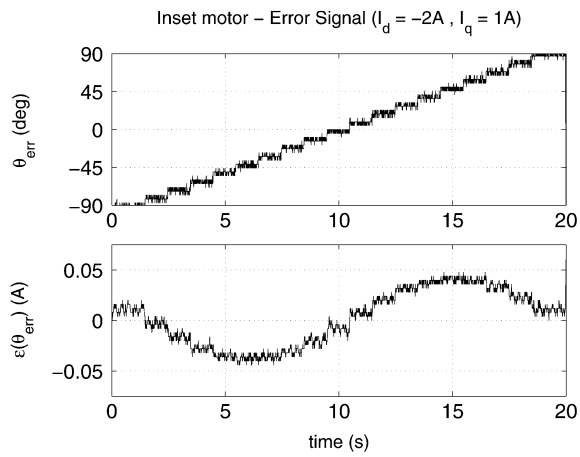

Fig. 13. Inset rotor: rotor position error and estimation error signal with pulsating voltage injection (experimental test).

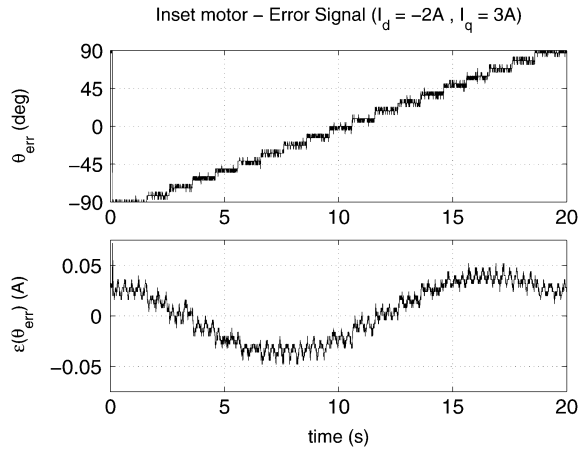

Fig. 14. Inset rotor: rotor position error and estimation error signal with pulsating voltage injection (experimental test).

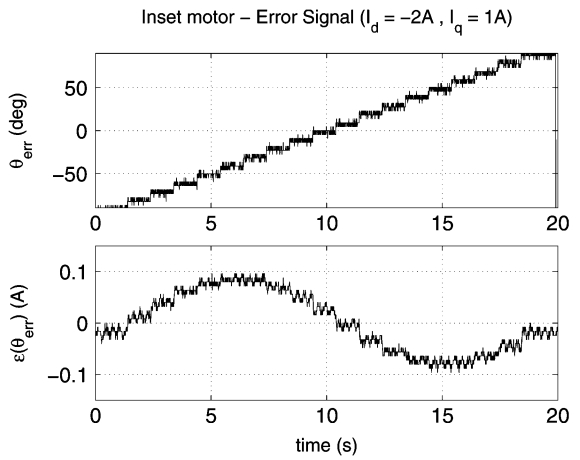

Fig. 15. Inset rotor: rotor position error and estimation error signal with rotating voltage injection (experimental test).

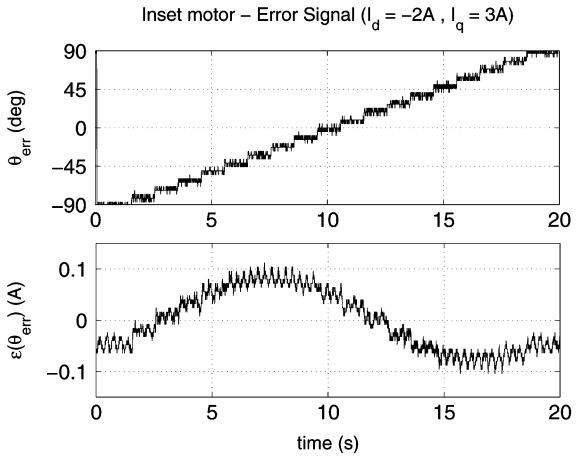

Fig. 16. Inset rotor: rotor position error and estimation error signal with rotating voltage injection (experimental test).

error signal is higher in simulations, the behavior with the fundamental current is the same.

C. Pulsating Voltage Vector (Inset Motor Configuration)

The measurements on the inset motor with pulsating voltage injection are reported in Fig. 13 (low current test) and Fig. 14 (high current test). The error signal with $I_q = 0$ A is similar to that of Fig. 13 and it is not reported here. From Fig. 14, it is worth noticing that the rotor position of the inset motor can be detected also when a q-axis current is higher than $I_q = 3$ A.

However, the effect of the d- and q-axis cross-coupling is evident by the shifting of the sinusoidal waveform. The experimental results of Figs. 13 and 14 can be compared with the predicted results of Fig. 7. In this case, a good agreement between the two results is evident. The absence of small saturable parts (as the rotor iron bridges of the IPM rotor) makes the FE model very accurate.

D. Rotating Voltage Vector (Inset Motor Configuration)

Some measurements on the inset motor are reported in Fig. 15 (according to a low fundamental current) and Fig. 16 (according to a high fundamental current).

Also in this case, one can observe that the rotor position of the inset motor can be detected for a q-axis current higher than $I_q = 3$ A, even though an angular shifting occurs in the error signal.

Results of Figs. 15 and 16 can be compared with those of Fig. 8. As above a good match between measurements and predictions is achieved.

E. Measures of Inset Motor With Very High Currents

Fig. 17 shows the rotor position estimation error signal measured at very high fundamental q-axis current, adopting pulsating voltage injection. Similarly, Fig. 18 shows the same signal measured adopting rotating voltage injection. These measures again match the predictions of Figs. 7 and 8.

From these tests two considerations are worth noticing. At first the incremental saliency ratio decreases slightly, so that the rotor position estimation error signal can be detected also at these high currents. Second, high angular shifting can be observed. It causes an incorrect rotor position detection: the zero of the error signal ε does not correspond to the zero of the signal $\vartheta^e_{\rm err}$.

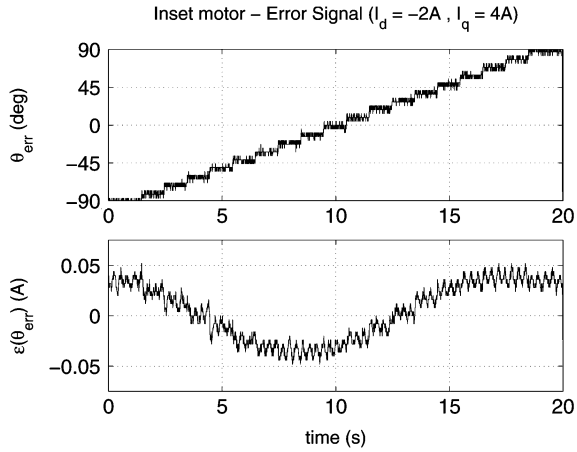

Fig. 17. Inset rotor: rotor position error and estimation error signal with pulsating voltage injection (experimental test).

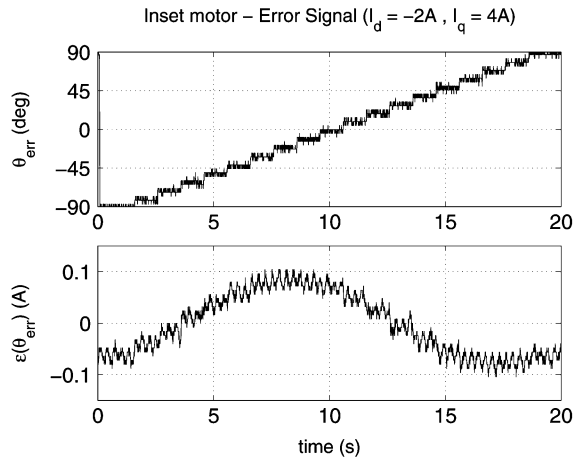

Fig. 18. Inset rotor: rotor position error and estimation error signal with rotating voltage injection (experimental test).

In any case, the first consideration implies that inset motor is more advantageous than the IPM motor. In fact, when IPM motor is working at high currents, the error signal is lost, while this does not happen in inset motor. The angular shifting that occurs at high currents is a drawback for the rotor position detection. However, the angular shifting can be compensated in the control, in order to operate the motor even at high currents.

F. Discussion

From the tests presented above, a substantial difference between the two techniques has not be found. Conversely, the two motors exhibit a very different response to the same injected high-frequency signal.

The reason of this different behavior of the two motors can be imputed to the different magnetic loadings of the two machines. In the IPM motor, the magnetic loading under load tends to saturate the rotor paths, as shown in Fig. 19(a). Since the rotor is the salient part of the machine, the saturation decreases the magnetic saliency between the d- and the q-axis, thus the high-frequency signal decreases to zero.

Conversely, in the inset motor the magnetic loading under load tends to saturate the stator paths, as shown in Fig. 19(b).

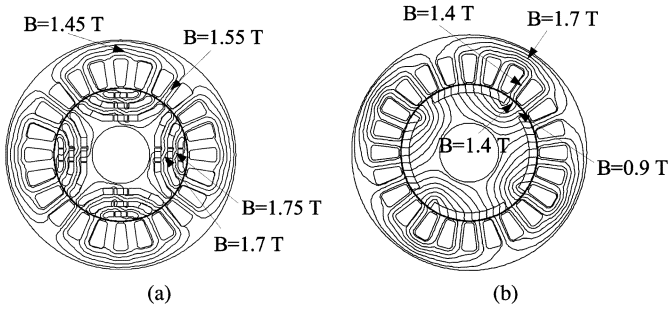

Fig. 19. Flux plot under rated load (a) IPM rotor and (b) inset rotor.

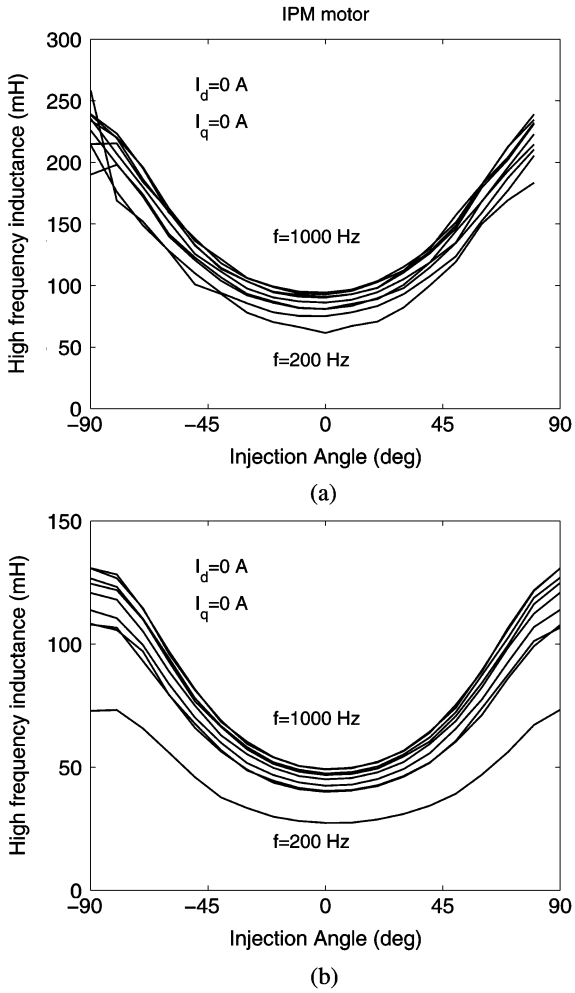

Fig. 20. High-frequency inductance versus angle of the injected signal with (a) IPM rotor and (b) inset rotor.

In this case the salient part of the machine (the rotor) remains almost unsaturated. The magnetic saliency is slightly influenced by the saturation and the amplitude of the high-frequency signal remains almost unchanged. However, the saturation of the stator modifies the flux lines according to the current amplitude, and causes the angular shifting that is observed in the rotor position detection.

As regards the effect of the variation of the frequency of the injected signal, since both rotors are laminated there is a minimum impact. Fig. 20 shows the incremental inductance versus

the angle of the injected signal, for different values of its frequency, from 200 and 1000 Hz. The influence on the detected inductance is minimum for both rotors.

VI. Conclusion

This paper presents an overall comparison between motor configurations and high-frequency voltage injection techniques. It investigates the response to a high-frequency voltage injection of two rotor configurations: an IPM rotor with three flux-barriers per pole and an inset rotor, with iron teeth separating the adjacent surface-mounted PMs. Both high-frequency pulsating and rotating voltage injection techniques are used to detect the rotor position angle.

The effectiveness of the rotor position detection is investigated under several operating conditions, which means for various torque requirements. Fundamental d- and q-axis currents are varied.

This comparison has been carried out using both simulations and experiments. In the first case, a finite element analysis is carried out to compute the d- and q-axis flux linkages as a function of the d- and q-axis currents. This magnetic model is used to simulate the motor response to a high-frequency signal. In the second case a high-frequency voltage signal is injected in actual motors. The appreciable agreement between the two methods confirms the goodness of the simulation approach.

As far as the high-frequency voltage injection techniques, it has been observed that there is not a substantial difference between the two techniques. When the torque requirement is high, the estimation error signal is lost or highly distort. However, only static performance have been compared and some differences could be observed comparing dynamic responses.

On the contrary, the comparison between the two motors shown that the rotor position of the inset rotor can be detected at a higher q-axis currents (i.e., under a higher load), in comparison with the IPM motor. Although a shifting of the rotor position estimation error signal is observed at the higher loads, the incremental saliency remains. Since both rotors adopt laminations, it was also observed that carried frequency does not affect the results.

Acknowledgment

The authors wish to thank Dr. G. Teruzzi, Saimag. S.p.a., Pogliano Milanese, Italy, for the permanent magnets used in the rotors.

References

[1] S. Morimoto, K. Kawamoto, M. Sanada, and Y. Takeda, "Sensorless control strategy for salient-pole PMSM based on extended EMF in rotating reference frame," *IEEE Trans. Ind. Appl.*, vol. 38, no. 4, pp. 1054–1061, Jul./Aug. 2002.

[2] S. Bolognani, M. Zigliotto, and M. Zordan, "Extended-range pmsm sensorless speed drive based on stochastic filtering," *IEEE Trans. Power Electron.*, vol. PE–16, no. 1, pp. 110–117, Jan. 2001.

[3] N. R. Patel, T. O'Meara, J. Nagashima, and R. D. Lorenz, "Encoderless interior permanent magnet traction drive for electrical and hybrid electrical vehicles," in *Proc. IEEE Ind. Appl. Soc. Annu. Meeting*, , Sep. 30–Oct. 5 2001, pp. 1703–1707.

[4] B. J. Brunsbach, G. Henneberger, and T. Klepsch, "Position controlled, permanent excited synchonous motor without mechanical sensors," in *Proc. EPE Conf.*, Brighton, UK, Sep. 1993, pp. 38–43.

[5] P. L. Jansen and R. D. Lorenz, "Transducerless field orientation concepts employing saturation-induced saliencies in induction machines," *IEEE Trans. Ind. Appl.*, vol. 32, no. 6, pp. 1380–1393, Nov./Dec. 1996.

[6] A. B. Kulkarni and M. Ehsani, "A novel position sensor elimination technique for interior permanent-magnet synchronous drive," *IEEE Trans. Ind. Appl.*, vol. 28, no. 1, pp. 144–150, Jan./Feb. 1992.

[7] J. Kim and S. K. Sul, "New standstill position detection strategy for pmsm drive without rotational transducers," in *Proc. IEEE APEC Conf.*, Jun. 1994, pp. 363–369.

[8] S. Ogasawara and H. Akagi, "An approach to real-time position estimation at zero and low speed for a PM motor based on saliency," *IEEE Trans. Ind. Appl.*, vol. 34, no. 1, pp. 163–168, Jan./Feb. 1998.

[9] Y. S. Jeong, R. D. Lorenz, T. M. Jahns, and S. K. Sul, "Initial rotor position estimation of an IPM synchronous machine using carrier-frequency injection methods," *IEEE Trans. Ind. Appl.*, vol. IA-40, no. 1, pp. 38–45, Jan./Feb. 2005.

[10] N. Bianchi, S. Bolognani, and M. Zigliotto, "Design hints of an IPM synchronous motor for an effective position sensorless control," in *Proc. IEEE Power Electron. Spec. Conf (PESC'05)*, Recife, Brazil, Jun. 2005, pp. 1560–1566.

[11] G.-B. Kang, J.-H. Jung, H.-B. Ihm, and H.-G. Kim, "Initial rotor angle and parameter estimation scheme for IPM synchronous motor in hybrid electric vehicle at standstill," in *Proc. IEEE 35th Annu. Power Electron. Spec. Conf. (PESC'04)*, Jun. 20–25, 2004, vol. 5, pp. 4006–4009.

[12] A. Consoli, G. Scarcella, and A. Testa, "Sensorless control of PM synchronous motors at zero speed," in *Proc. 34th IEEE Ind. Appl. Soc. Annu. Meeting*, Phoenix, AZ, Oct. 3–7, 1999, vol. 2, pp. 1033–1040.

[13] A. Consoli, G. Scarcella, and A. Testa, "A new zero frequency flux position detection approach for direct field oriented control drives," *IEEE Trans. Ind. Appl.*, vol. 36, no. 3, pp. 797–804, May/Jun. 2000.

[14] F. Briz, A. Diez, and M. W. Degner, "Dynamic operation of carrier signal injection based sensorless, direct field oriented ac drives," *IEEE Trans. Ind. Appl.*, vol. 36, no. 5, pp. 1360–1368, Sep./Oct. 2000.

[15] J. Ha, K. Ide, T. Sawa, and S. K. Sul, "Sensorless rotor position estimation of an interior permanent-magnet motor from initial states," *IEEE Trans. Ind. Appl.*, vol. IA-39, no. 3, pp. 761–767, May 2003.

[16] J. H. Jang, J. I. Ha, M. Ohto, K. Ide, and S. K. Sul, "Analysis of permanent magnet machine for sensorless control based on high frequency signal injection," *IEEE Trans. Ind. Appl.*, vol. 40, no. 6, pp. 1595–1604, Nov./Dec. 2004.

[17] H. Kim and R. D. Lorenz, "Carrier signal injection based sensorless control methods for IPM synchronous machine drives," in *Proc. IAS'04*, Seattle, WA, Oct. 2004, vol. 2, pp. 977–984.

[18] A. Vagati, M. Pastorelli, and G. Franceschini, "Effect of cross-coupling in synchronous reluctance motors," in *Proc. Intell. Motion Conf.*, 1997, pp. 279–285.

[19] A. Vagati, M. Pastorelli, G. Franceschini, and S. C. Petrache, "Design of low-torque-ripple synchronous reluctance motors," *IEEE Trans. Ind. Appl.*, vol. IA-34, no. 4, pp. 758–765, Jul./Aug. 1998.

[20] A. Vagati, M. Pastorelli, G. Franceschini, and F. Scapino, "Impact of cross saturation in synchronous reluctance motors of transverse-laminated type," *IEEE Trans. Ind. Appl.*, vol. IA-36, no. 4, pp. 1039–1046, Jul./Aug. 2000.

[21] P. Guglielmi, M. Pastorelli, and A. Vagati, "Impact of cross-saturation in sensorless control of transverse-laminated synchronous reluctance motors," *IEEE Trans. Ind. Electron.*, vol. 53, no. 2, pp. 429–439, Apr. 2006.

[22] R. D. Lorenz and K. Van Patten, "High resolution velocity estimation for all digital, ac servo drives," *IEEE Trans. Ind. Appl.*, vol. 27, no. 4, pp. 701–705, Jul./Aug. 1991.

[23] M. Harke, H. Kim, and R. D. Lorenz, "Sensorless control of interior permanent magnet machine drives for zero-phase-lag position estimation," *IEEE Trans. Ind. Appl.*, vol. IA-39, no. 12, pp. 1661–1667, Nov./Dec. 2003.

[24] M. Linke, R. Kennel, and J. Holtz, "Sensorless speed and position control of synchronous machines using alternating carrier injection," in *Proc. Int. Elect. Mach. Drives Conf. (IEMDC'03)*, Madison, WI, 2–4 Jun. 2003, pp. 1211–1217.

[25] A. Consoli, G. Scarcella, G. Tutino, and A. Testa, "Sensorless field oriented control using common mode currents," in *Proc. Ind. App. Conf.*, Rome, Italy, Oct. 8–12, 2000, vol. 3, pp. 1866–1873.

[26] J. H. Jang, S. K. Sul, and Y. C. Son, "Current measurement issues in sensorless control algorithm using high frequency signal injection method," in *Proc. IEEE Ind. App. Soc. Annu. Meeting*, Salt Lake City, UT, Oct. 2003, pp. 1134–1141.

[27] F. Briz, M. W. Degner, A. Diez, and R. D. Lorenz, "Measuring, modeling, and decoupling of saturation-induced saliencies in carrier signal injection-based sensorless ac drives," *IEEE Trans. Ind. Appl.*, vol. 37, no. 5, pp. 1356–1364, Sep./Oct. 2001.
[28] F. Briz, M. W. Degner, A. B. Diez, and R. D. Lorenz, "Static and dynamic behavior of saturation-induced saliencies and their effect on carrier signal based sensorless ac drives," *IEEE Trans. Ind. Appl.*, vol. IA-38, no. 3, pp. 670–678, May/Jun. 2002.
[29] J. I. Ha, M. Ohto, J. H. Jang, and S. K. Sul, "Design and selection of ac machines for saliency-based sensorless control," in *Proc. IEEE Ind. Appl. Soc. Annu. Meeting*, Pittsburgh, PA, Oct. 2002, vol. 2, pp. 1155–1162.
[30] N. Bianchi, "Electrical Machine Analysis using Finite Elements," in *Power Electronics and Applications Series*. Boca Raton, FL: CRC, 2005.
[31] P. Guglielmi, M. Pastorelli, and A. Vagati, "Cross saturation effects in IPM motors and related impact on zero-speed sensorless control," *IEEE Trans. Ind. Appl.*, vol. 42, no. 6, pp. 1516–1522, Nov./Dec 2006.
[32] N. Bianchi and S. Bolognani, "Influence of rotor geometry of an interior PM motor on sensorless control feasibility," in *Proc. IEEE 40th Ind. Appl. Soc. Annu. Meeting (IAS'05)*, Hong Kong, Oct. 2005, vol. 4, pp. 2553–2560.

Nicola Bianchi (M'98) received the Laurea and Ph.D. degrees in electrical engineering from the University of Padova, Padova, Italy, in 1991 and 1995 respectively.

Since 1998, he has worked at the Department of Electrical Engineering, University of Padova, as a Senior Research Assistant in the Electric Drives Laboratory. He is author and coauthor of several technical papers and two books. His interest is in the field of the electromechanical design of brushless, synchronous and induction motors with particular interest to the drives applications.

Silverio Bolognani (M'98) received the Laurea degree in electrical eng. from University of Padova, Padova, Italy, in 1976.

In the same year, he joined the Department of Electrical Engineering. He is presently a Full Professor of electrical drives and he is engaged in research on advanced control techniques for motor drives and on the design of ac electrical motors for variable speed applications. He is author of more than 100 papers on electrical machines and drives.

Dr. Bolognani is the President of the IEEE IAS-IES-PELS North Italy Joint Chapter.

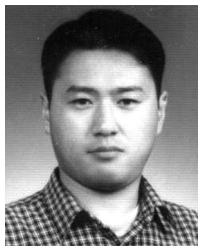

Ji-Hoon Jang (S'01) was born in Seoul, Korea, in 1975. He received the B.S., M.S., and Ph.D. degrees in electric engineering from Seoul National University, Seoul, Korea, in 1999, 2001, and 2006, respectively.

He was a Visiting Scholar with the Center for Power Electronics Systems (CPES), Bradley Department of Electrical and Computer Engineering, Virginia Polytechnic Institute and State University, Blacksburg, from September 2003 to September 2004, where he was working on the control of PM machines for starter/generator and electric pump/fan applications in aircraft systems. He is currently a Senior Research Engineer at the Hybrid System Engineering Team, R&D Center, Hyundai Motor Company, Gyeonggi-Do, Korea. His current research interests are high-performance ac machine drives including position sensorless controls and electric vehicle drives.

Seung-Ki Sul (S'78–M'80–SM'98–F'00) was born in Korea in 1958. He received the B.S., M.S., and Ph.D. degrees in electrical engineering from Seoul National University, Seoul, Korea, in 1980, 1983, and 1986, respectively.

From 1986 to 1988, he was an Associate Researcher with the Department of Electrical and Computer Engineering, University of Wisconsin, Madison. From 1988 to 1990, he was a Principal Research Engineer with Gold-Star Industrial Systems Company. Since 1991, he has been a member of the faculty of the School of Electrical Engineering, Seoul National University, where he is currently a Professor. His current research interests are power-electronic control of electric machines, electric/hybrid vehicle drives, and power-converter circuits.